



# Cytological effects of honokiol treatment and its potential mechanism of action in non-small cell lung cancer



Jie Zhang<sup>1</sup>, Yueming Zhang<sup>1</sup>, Wen Shen, Ran Fu, Zongli Ding, Yulong Zhen\*, Yufeng Wan\*

Department of Respiratory Diseases, The Affiliated Huai'an Hospital of Xuzhou Medical University, Huai'an 223002, China

## ARTICLE INFO

**Keywords:**  
Non-small cell lung cancer  
Apoptosis  
miR-148a-3p  
Let-7c-5p  
Prognosis

## ABSTRACT

**Purpose:** In this study, we aimed to explore key micro(mi)RNAs and their potential regulatory mechanisms induced by honokiol treatment in non-small cell lung cancer (NSCLC) cells.

**Methods:** NSCLC A549 cells were treated with 0 (control) or 45 μM honokiol. Cell proliferation and migration were determined using CCK-8 and transwell assay, respectively, and apoptosis was determined using flow cytometry. RNA-sequencing was performed to detect the transcript expression levels. The differentially expressed miRNAs (DE-miRNAs) between the honokiol group and the control group were screened and analyzed for their functions and pathways. Then, protein-protein interaction (PPI) networks and miRNA-mRNA regulatory networks were constructed. In addition, survival analysis based on the key miRNAs was performed. Finally, the expression of the key miRNAs and their target genes were determined, and their effects on drug sensitivity were validated using their inhibitors.

**Results:** Cell proliferation and migration were inhibited ( $P < 0.01$ ), and the apoptosis rate was increased ( $P < 0.01$ ) after honokiol treatment compared to that in the control group. A total of 26 upregulated and 20 downregulated DE-miRNAs were screened. DE-miRNAs were enriched in 10 pathways and 48 biological processes, such as the PI3K/AKT signaling pathway (involving miR-148a-3p). The miRNA-mRNA regulatory networks involved eight upregulated (including miR-148a-3p and let-7c-5p) and seven downregulated miRNAs (including miR-7-5p) and 190 target mRNAs. Survival analysis revealed that let-7c-5p, miR-148a-3p, and miR-148a-5p levels correlated with NSCLC prognosis. The expression of let-7c-5p, miR-148a-3p, and miR-148a-5p was significantly increased and negatively correlated with the expression of their target genes. The cytological effects of honokiol on A549 cells was partly reversed by treatment with the inhibitors of Let-7c-5p and miR-148a-3p.

**Conclusion:** Let-7c-5p, miR-148a-3p, miR-148a-5p, and miR-7-5p are favorable indicators of NSCLC patients treated with honokiol.

## 1. Introduction

Lung cancer is a common malignant tumor and a major cause of cancer-related deaths worldwide. About 85% of lung cancer cases are diagnosed as non-small cell lung cancer (NSCLC) [1]. Squamous-cell carcinoma, adenocarcinoma, and large-cell lung cancer are the three major subtypes of NSCLC [2]. The diagnoses of most patients with NSCLC are confirmed at the middle or terminal stage, resulting in a low survival rate of 5 years [3]. The identification of accurate biomarkers for early diagnosis and therapeutic targets is necessary to improve the outcomes of NSCLC.

In recent years, there have been several studies on the role of microRNAs (miRNAs) in lung cancer. Precise tumor classification is a

prerequisite for targeted therapy of NSCLC. Reportedly, miRNA expression profiles can be used to distinguish lung cancers from non-cancerous lung tissues as well as determine the histological subtypes of lung cancer [4]. miRNAs can therefore act as clinical biomarkers for the early diagnosis and prognosis of lung cancer, and are related to metastasis and patient survival [5]. In addition, miRNAs can directly target oncogenes or tumor suppressor genes to mediate the progression of tumors [6]. Charkiewicz et al. reported that the expression levels of miR-205 and miR-21 could reliably determine the subtype of NSCLC [7]. The expression of miR-205 and miR-21 in patients with NSCLC was found to be significantly increased, and the overexpression of miR-21 has been shown to be associated with a negative prognosis for the overall survival of patients [8]. In addition, miR-21, miR-17, and miR-

\* Corresponding authors.

E-mail addresses: [ha183@163.com](mailto:ha183@163.com) (Y. Zhen), [ggwanyufeng@163.com](mailto:ggwanyufeng@163.com) (Y. Wan).

<sup>1</sup> These authors contributed equally to this work.

192 are specifically expressed in NSCLC and function as indicators for the early diagnosis of NSCLC [9,10]. miR-196a promotes the proliferation and invasion of A549 cells by targeting Homeobox A5 [11]. These biomarkers provide new opportunities for the discovery of novel drug targets and the development of therapeutic strategies.

Honokiol is a small molecular-weight polyphenol that can inhibit angiogenesis and tumor growth [12]. Pearson demonstrated that co-treatment with cetuximab and honokiol reduced cell proliferation and induced apoptosis in cetuximab-resistant clones by downregulating the HER family genes and MAPK and AKT signaling pathways [13]. Honokiol significantly inhibited NSCLC cell growth and increased G1 phase arrest and apoptosis by suppressing the expression of class I histone deacetylase via proteasomal degradation [14]. Honokiol induces G1 phase arrest and apoptosis of NSCLC cells harboring mutant KRAS by interfering with the KRAS-mediated RAF/PI3K/AKT signaling pathway, and triggers autophagy via the Sirt3/Hif-1 $\alpha$  pathway [15]. Although honokiol has been reported to inhibit cell growth and induce apoptosis in NSCLC cells, the potential role of the miRNAs involved and their underlying regulatory mechanisms have not yet been elucidated.

In this study, we performed high-throughput sequencing on honokiol-treated NSCLC A549 cells to identify differentially expressed miRNAs (DE-miRNAs). Then, functional enrichment analysis and survival analysis based on the DE-miRNAs were performed, and the DE-miRNA target genes were predicted to determine the regulatory relationship. Thus, we attempted to elucidate the potential molecular regulatory mechanisms underlying the action of honokiol in NSCLC cells.

## 2. Material and methods

### 2.1. Cell culture

NSCLC cell lines A549 were purchased from the Cell Bank of the Chinese Academy of Sciences (Shanghai, China). The cells were cultured in RPMI-1640 medium (catalog no. 31985-070, Gibco) supplemented with 10% fetal bovine serum (FBS, catalog no. 10099-141, Gibco) and 1% penicillin-streptomycin (catalog no. 15140-122, Gibco) in an incubator with 5% CO<sub>2</sub> at 37 °C.

### 2.2. Cell treatments and cell counting kit-8 (CCK-8) assay

The A549 cells were plated in 96-well plates at a density of  $1.0 \times 10^3$  cells/well and cultured overnight at 37 °C with five repeats for each group. When the cells reached 30–50% confluency, they were treated with 0, 5, 10, 20, 40, 80, and 100  $\mu$ M honokiol (catalog no. 35354-74-6, MCE) and incubated for 24 h and 48 h under 5% CO<sub>2</sub> at 37 °C. Then, 10  $\mu$ L of 5 mg/mL CCK-8 solution (catalog no. C0039, Beyotime, Shanghai, China) was added to each well and the cells were incubated for 1 h in dark conditions. Subsequently, the optical density (OD) of each well at 450 nm was detected using TECAN (Infinite M100 PRO, Tecan Group Ltd., Mannedorf, Switzerland). Based on the results of the CCK-8 assay, the treatment conditions were 45  $\mu$ M honokiol treatment for 48 h on NSCLC A549 cells for further analysis.

### 2.3. miRNA inhibitors and cell transfection

miRNA inhibitors were synthesized by GenePharma (Shanghai, China). The miRNA inhibitors of miR-148a-3p and let-7c-5p (diluted in 200  $\mu$ L serum-free Opti-MEM medium) were transfected to A549 cells using Lipofectamine 2000 (catalog no. 11668019, Invitrogen), according to the manufacturer's instructions.

### 2.4. Cell migration assay

One hundred microliters of A549 cell culture ( $5 \times 10^6$  cells/mL) were placed on the upper layer of a cell culture containing serum-free

medium supplemented with honokiol, and 500  $\mu$ L fresh complete medium was placed below the cell permeable membrane in an incubator under 5% CO<sub>2</sub> at 37 °C. After 48 h of incubation, cell migration was detected by crystal violet staining. Briefly, the cells were washed with PBS three times after incubating for 48 h. Then, 4% paraformaldehyde was used to fix the cells for 20–30 min. The cells were then stained with crystal violet for 10 min after washing with PBS three times. Finally, PBS was used to remove the crystal violet, and cell migration was observed under a microscope.

### 2.5. Apoptosis analysis

A549 cells were placed in a six-well plate at a density of  $2 \times 10^5$  cells/mL and cultured overnight. On the second day, the cells were treated with 0  $\mu$ M (control group) and 45  $\mu$ M honokiol when the cell density reached 30–50% confluency, with five repeats for each group. After treatment for 48 h, the cells were digested with 0.25% trypsin and centrifuged at 300  $\times$ g for 3 min. Then, the cells were resuspended and incubated in 100  $\mu$ L 1 $\times$  binding buffer, 5  $\mu$ L FITC-Annexin-V (catalog no. 40301ES50, BD), and 5  $\mu$ L of 50  $\mu$ g/mL propidium iodide (Sigma), in dark conditions at room temperature for 15 min. Finally, 400  $\mu$ L of 1 $\times$  binding buffer was added to each well and cell apoptosis was measured using the FACS Calibur flow cytometer (BD).

### 2.6. Cell preparation for RNA-sequencing and reverse transcription quantitative PCR (RT-qPCR)

A549 cells were plated in a six-well plate at a density of  $2 \times 10^5$  cells/mL,

cultured overnight, and treated with 0  $\mu$ M (control group) and 45  $\mu$ M honokiol once the cells reached 30–50% confluency. Three samples were treated in each group (treatment group: case1, case2, and case3; control group: Ctrl1, Ctrl2, and Ctrl3). After 48 h of cultivation, the cells in the two groups were harvested for RNA-sequencing and RT-qPCR (samples were stored at  $-80$  °C before RT-qPCR).

### 2.7. RNA extraction and sequencing

Total RNA was extracted using TRIzol (Invitrogen; Thermo Fisher Scientific, Inc), according to the manufacturer's instructions. The quality and concentration of the total RNA were determined using a microplate reader (Infinite M100 PRO, TECAN). Then, total RNA (1  $\mu$ g/sample) was reverse-transcribed to construct a cDNA library using NEXTflex™ Small RNA-Seq Kit v3 (Illumina), according to the manufacturer's instructions, and the cDNAs were amplified by 11–12 cycles of PCR reaction. Then, the mRNAs were purified using 6% Novex TBE PAGE gel (Invitrogen; Thermo Fisher Scientific, Inc). The concentration of cDNAs in the library was measured using Quantus™ Fluorometer QuantiFluor® dsDNA System (Promega). cDNA libraries were merged based on the data size and valid cDNA concentration, and cDNA library clusters were then created using an Illumina cBot. Finally, the cDNA libraries were sequenced on an Illumina HiSeq™ 4000 (Illumina, Inc., San Diego, CA, USA).

### 2.8. Pretreatment of RNA-sequencing data

Sample quality and read numbers were assessed using FASTQC. For all generated raw reads, the selection criteria were employed to remove the unreliable reads to ensure the accuracy of subsequent analysis. The selection criteria were as follows: (1) remove the paired reads with adapter; (2) remove the paired reads when the number of N > 10% bases of this read; and (3) remove the paired reads when the number of low quality bases (Q  $\leq$  5) is more than 50% bases of this read. As a result, the final data included only the clean reads. The Bowtie package [16] was used to align the clean reads to a reference genome (GRCh38) using default parameters. The HTSeq-count (v0.9.1) was used

independently to obtain the read counts based on human miRNA annotations downloaded from miRBase.

## 2.9. Distance analysis and principal component analysis (PCA)

The correlation between expression levels of miRNAs between the samples is an important index to evaluate the reliability of the experiment and the rationale behind sample selection. Here, the dispersion relationship between the samples and the PCA was examined to assess the correlation between samples based on the normalization of expression level with the Deseq2 package [17] (version 1.12.4, <https://bioconductor.org/packages/release/bioc/html/DESeq2.html>). A lower value of dispersion relationship represented a higher similarity of expression patterns between the samples. The Prcomp function was used to reduce the dimension of the data, and the plotPCA function in the Deseq2 package was used to construct a PCA diagram.

## 2.10. DE-miRNA screening

The DE-miRNAs between the honokiol and control groups were screened using Wald's negative binomial test based on the Deseq2 package, and the Benjamini-Hochberg method was utilized to conduct the false discovery rate correction. The DE-miRNAs with threshold values of  $P_{adj} < 0.01$  and  $|\log \text{ fold change (FC)}| > 0.585$  were screened to perform the subsequent analysis.

## 2.11. DE-miRNA target gene prediction

The DE-miRNA target gene prediction was performed using the miRNA-Gene Targets of miRWalk 2.0 (<http://zmf.umm.uni-heidelberg.de/apps/zmf/mirwalk2/miRreys-self.html>) using the following parameter settings: select database, miRBase; species, human; other databases, miRWalk, miRDB, miRNAMap, RNAhybrid, RNA22, miRanda, and Targetscan; retrieval relation, AND. The target genes present in all the seven databases were selected.

## 2.12. Function and pathway enrichment analysis of DE-miRNAs

The Kyoto Encyclopedia of Genes and Genomes database (KEGG) [18] pathway and gene ontology (GO) [19] annotation enrichment analysis for the DE-miRNAs with more than five target genes were conducted using the clusterProfiler in R package (version 3.2.11, <http://www.bioconductor.org/packages/release/bioc/html/clusterProfiler.html>). The significantly enriched pathways and GO annotations were selected using the threshold of  $p\text{-value} < 0.01$ .

## 2.13. Construction of regulatory network

Search Tool for the Retrieval of Interacting Genes [20] (STRING, version 10.0, <http://www.string-db.org/>) was used to retrieve the protein-protein interactions (PPI) among the target genes using the following parameters: species, homo; PPI score, 0.4. Cytoscape [21] (version 3.4.0, <http://chianti.ucsd.edu/cytoscape-3.4.0/>) was used to construct the PPI network based on the interactions retrieved from STRING analysis; in addition, the Cytonca plugin [22] (version 2.1.6, <http://apps.cytoscape.org/apps/cytonca>) was used to analyze the topology of the nodes in the PPI network with the parameter setting as "without weight." Finally, the regulatory network was constructed combining the miRNA-Target interactions and PPI network.

## 2.14. Survival analysis based on key DE-miRNAs

The survival data for lung adenocarcinomas (LUAD) in The Cancer Genome Atlas (TCGA) was downloaded from the University of California Santa Cruz [23] (UCSC, <http://xena.ucsc.edu/>) Genome Browser database, which contained clinical outcomes (including overall

survival (OS) and OS status) and miRNA-mature-seq data. A total of 435 LUAD samples with survival data were obtained by sample one-to-one correspondence. The DE-miRNAs were split into low expression and high expression groups according to the median value of expression values abstracted from TCGA. The log-rank statistical test was conducted with the threshold of  $p\text{-value} < 0.05$ , and the Kaplan-Meier (K-M) survival curve was plotted by analyzing the associations between the miRNAs and prognosis.

## 2.15. RT-qPCR

Total RNA extraction was conducted using TRIzol reagent (Invitrogen; Thermo Fisher Scientific, Inc), according to the manufacturer's instructions. The quality and concentration of the total RNA were measured using a microplate reader (Infinite M100 PRO, TECAN). The total RNA was reverse transcribed using PrimeScript™RT Master Mix (No. RR036A, Takara, Japan). Then, RT-qPCR was carried out using Power SYBR Green PCR Master Mix (No. A25742, Thermo Scientific, MA, USA) to determine the gene expression level. The thermal cycling conditions were as follows: 50 °C for 3 min, 95 °C for 3 min, followed by 40 cycles at 95 °C for 10 s and 60 °C for 30 s. The melting curve was analyzed from 60 °C to 95 °C at an incremental rate of 0.5 °C/10 s. The relative expression of the genes was calculated using the  $2^{-\Delta\Delta Ct}$  method [24]. The primer sequences for the genes were as follows: miR-148a-5p-RT, 5'-GTCGTATCCAGTGCAGGGTCCGAGGTATTCGCACTGGATACGACAGTCCG-3'; miR-148a-5p, forward 5'-GCGCAAAGTTCTGAGACACT-3'; let-7c-5p-RT, 5'-GTCGTATCCAGTGCAGGGTCCGAGGTATTCGCACTGGATACGACAACCAT-3'; let-7c-5p, forward 5'-GCGCTGAGGTAGTAGGTTGT-3'; miR-148a-3p-RT, 5'-GTCGTATCCAGTGCAGGGTCCGAGGTATTCGCACTGGATACGACAAAG-3'; miR-148a-3p, forward 5'-CGCTCAGTGCCTACAGAA-3'; universal reverse 5'-GTGCAGGGTCCGAGGT-3'; U6-RT, 5'-GTCGTATCCAGTGCAGGGTCCGAGGTATTCGCACTGGATACGACAAATATG-3'; U6, forward 5'-CTCGCTTCGGCAGCAC-3'; U6, reverse 5'-AACGCTTCACGAATTTGCGT-3'; Collagen Type III Alpha 1 Chain (COL3A1), forward 5'-GGAGCTGGCTACTTCTCGC-3'; COL3A1, reverse 5'-GGGAACATCTCTCTCAACAG-3'; Integrin Subunit Alpha 5 (ITGA5), forward 5'-GCTGTGGAGTACAAGTCCTT-3'; ITGA5, reverse 5'-AATTCGGGTGAAGTTATCTGTGG-3'; ErbB2 Receptor Tyrosine Kinase 3 (ERBB3), forward 5'-GGTATGGGGAACTTGAGAT-3'; ERBB3, reverse 5'-CTGTCACTTCTCGAATCCACTG-3'; GAPDH, forward 5'-TGACAACCTTGGTATCGTGGAAAG-3'; GAPDH, reverse 5'-AGGCAGGGATGATGTTCTGGAGAG-3'.

## 2.16. Statistical analysis

Data are presented as the means  $\pm$  standard deviation (SD). The software Graphpad Prism 5 (Graphpad Software, San Diego, CA) was used to perform the statistical analysis. The method used for statistical analysis was the Student's t-test, where a  $p < 0.05$  was considered to represent a statistically significant difference.

## 3. Results

### 3.1. Honokiol suppressed proliferation and migration, and triggered apoptosis in A549 cells

Cell proliferation of honokiol-treated A549 cells was determined using the CCK-8 assay. The result showed that treatment with 0.45  $\mu\text{M}$  honokiol for 48 h significantly suppressed the proliferation of A549 cells ( $P < 0.01$ ) compared with that in the control group (Fig. 1). The migration of A549 cells was also significantly suppressed under 0.45  $\mu\text{M}$  honokiol treatment for 48 h ( $P < 0.01$ ) compared with that in the control group (Fig. 2A). Further, honokiol treatment for 48 h significantly enhanced ( $P < 0.01$ ) the apoptosis of A549 cells compared with that in the control group (Fig. 2B).

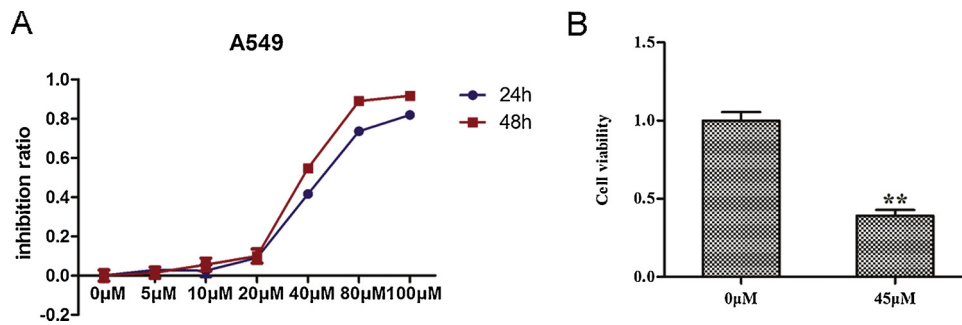


**Fig. 1.** Proliferation of honokiol-treated A549 cells analyzed by CCK-8 assay. A: The cell-viability-versus-honokiol-concentration curve; B: A549 cell proliferation significantly decreased compared with that in the control group,  $P < 0.01$ .

**3.2. Distance analysis and PCA results**

A total of 836 miRNAs were selected from the six samples after data preprocessing, and distance analysis and PCA using these samples were conducted. The results revealed significant differences in the samples of the treatment group compared with the control group (Fig. 3A–B).

**3.3. DE-miRNA screening and DE-miRNA target gene prediction**

Forty-six DE-miRNAs were identified between the honokiol and control groups, including 26 upregulated and 20 downregulated DE-miRNAs. Fig. 3C presents the heatmap for the DE-miRNAs, and shows that the expression of the DE-miRNAs could be significantly distinguished among the groups. In total, 211 DE-miRNA-target gene interactions were screened in the seven databases, and 15 DE-miRNAs and 190 mRNAs were obtained after the removal of repeats.

**3.4. Function and pathway enrichment of DE-miRNAs**

The function and pathway enrichment analysis for DE-miRNAs with more than five target genes is shown in Fig. 4. In total, six DE-miRNAs were significantly enriched in 10 pathways (Fig. 4A), including the PI3K-Akt signaling pathway (involving miR-148a-3p and miR-122-5p), nucleotide excision repair, and DNA replication. Furthermore, a total of 12 DE-miRNAs were significantly enriched in 48 GO terms (Fig. 4B), including core promoter binding, growth factor binding, and core promoter proximal region sequence-specific DNA binding.

**3.5. Regulatory network**

The PPI network of the DE-miRNA target genes consisted of 108 nodes and 128 interactions (Fig. 5A). The RB Transcriptional Corepressor 1 (RB1, degree = 11), Insulin Like Growth Factor 1 Receptor (IGF1R, degree = 9), Collagen Type I Alpha 2 Chain (COL1A2, degree = 7), Phosphoribosylformylglycinamide Synthase (PFAS,

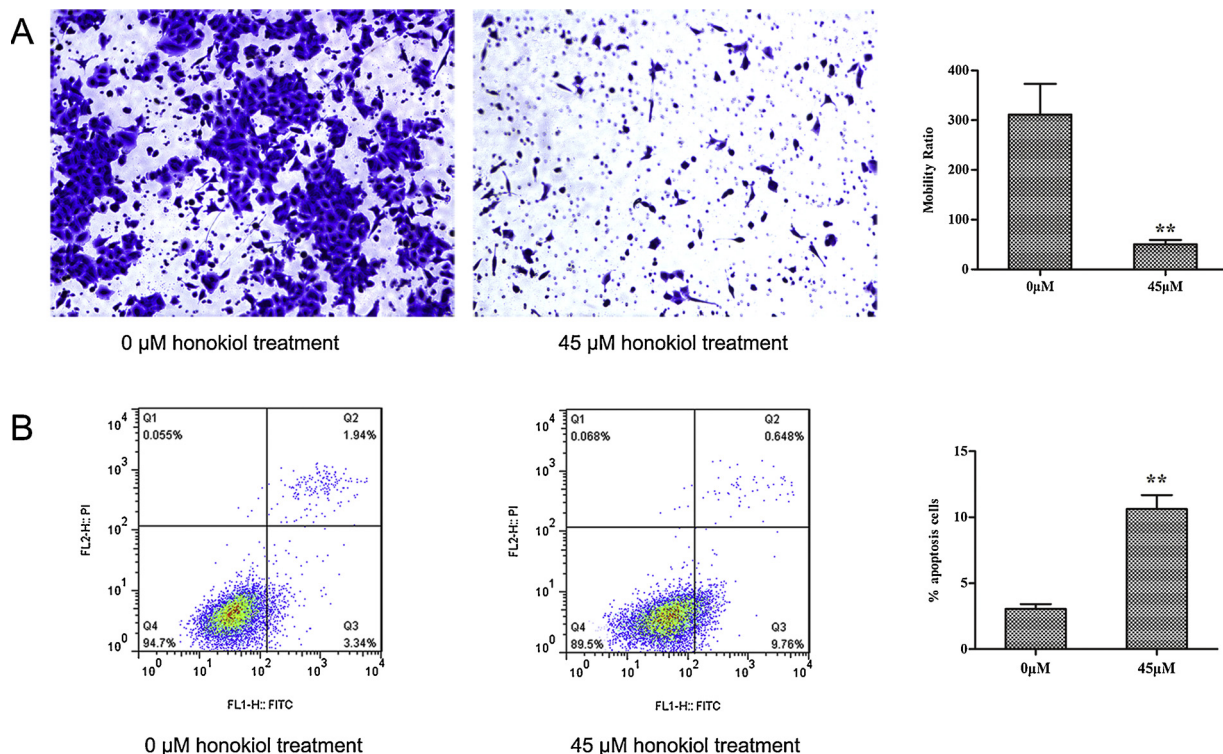


**Fig. 2.** Honokiol inhibited migration and induced apoptosis of A549 cells. A: Transwell assay was used to determine the migration of A549 cells. The migration of A549 cells was significantly reduced at 48 h compared with that in the control group,  $P < 0.01$ . B: Flow cytometry was conducted to determine the apoptosis of A549 cells. The apoptosis of A549 cells was significantly increased compared with that in the control group,  $P < 0.01$ .

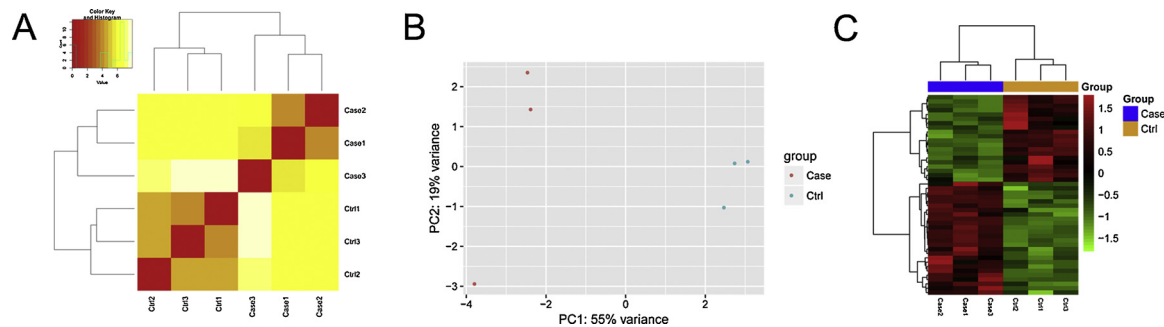


**Fig. 3.** Distance analysis and PCA among samples and heatmap for DE-miRNAs among different groups.

A: The heatmap of distance analysis among samples, B: PCA analysis of the samples. C: The heatmap of DE-miRNAs between the honokiol group and the control group. Case1-3 represent three replicate samples in the honokiol group. Ctrl1-3 represent three replicate samples in the control group. Red represents the upregulated DE-miRNAs, while blue represents the downregulated DE-miRNAs. PCA, principal component analysis.

degree = 6), and Kinesin Family Member 11 (KIF11, degree = 6) were the hub genes observed in the PPI network. The top 20 genes are presented in Table 1. The DE-miRNA-mRNA regulatory networks consisted of 205 nodes (15 DE-miRNAs and 190 mRNAs) and 339 interactions (Fig. 5B). There were seven downregulated DE-miRNAs and eight upregulated DE-miRNAs in the regulatory network, and the hub gene RB1 was regulated by miR-7-5p. The upregulated DE-miRNAs, let-7c-5p and miR-148a-3p, showed a high number of target genes; let-7c-5p regulated the COL3A1 and IGF1R genes, and miR-148a-3p regulated the ITGA5 and ERBB3 genes.

### 3.6. Survival based on key DE-miRNAs

The associations between miRNAs and prognosis were analyzed, and let-7c-5p, miR-148a-3p, and miR-148a-5p were observed to be associated with the prognosis of NSCLC. Let-7c-5p, miR-148a-5p, and miR-148a-3p were all significantly upregulated. The K-M survival curves of let-7c-5p, miR-148a-5p, and miR-148a-3p are shown in Fig. 6.

### 3.7. Expression of DE-miRNAs

Based on the bioinformatics analysis, the expression levels of let-7c-5p, miR-148a-5p, and miR-148a-3p, as well as their target genes were verified using RT-qPCR. The expression of let-7c-5p, miR-148a-5p, and miR-148a-3p was significantly upregulated (miR-148a-5p and miR-148a-3p,  $P < 0.01$ ; let-7c-5p,  $P < 0.05$ ) in the honokiol treatment group compared with that in the control group (Fig. 7A). These results were consistent with the results obtained by the bioinformatics analysis. The let-7c-5p target gene, COL3A1 ( $P < 0.01$ ), and the miR-148a-3p target genes, ITGA5 and ERBB3, were significantly downregulated in the honokiol treatment group compared with that in the control group (ERBB3,  $P < 0.01$ ; ITGA5,  $P < 0.05$ ) (Fig. 7B).

### 3.8. Let-7c-5p and miR-148a-3p inhibitors reversed the cytological effects of honokiol

To further confirm the effects of the key DE-miRNAs on drug sensitivity in A549 cells, the inhibitors of miR-148a-3p and miR-7c-5p were used to down-regulate their expression (Fig. 8A). Consistent with the findings above, apoptosis was clearly induced with honokiol treatment, while apoptosis was attenuated by the inhibitors of miR-148a-3p and miR-7c-5p, with a significant increase compared with that in the control (Fig. 8B). Similarly, the cell migration was significantly suppressed by honokiol treatment, and enhanced by the inhibitors of miR-148a-3p and miR-7c-5p, with a significant decrease compared with that in the control (Fig. 8C).

## 4. Discussion

In this study, the proliferation and migration of A549 cells were significantly inhibited, and their apoptosis was significantly enhanced after honokiol treatment. The bioinformatics analysis led to the identification of a total of 46 DE-miRNAs, including 26 upregulated and 20 downregulated DE-miRNAs. DE-miRNAs with more than five target genes were enriched in 10 KEGG pathways, including the PI3K/AKT signaling pathway (involving miR-148a-3p and its target genes ITGA5 and ERBB3), and the protein digestion and absorption pathway (involving miR-7c-5p and the target gene COL3A1), and were enriched in 48 biological processes, such as core promoter binding (involving miR-7-5p). RB1 was the hub gene with the greatest degree of interaction in the PPI network, and was regulated by miR-7-5p. The expression of the upregulated miRNAs, including let-7c-5p, miR-148a-5p, and miR-148a-3p, was significantly correlated with the prognosis of NSCLC. The expression of let-7c-5p and miR-148a-3p was negatively correlated with that of their target genes.

Human miRNA let-7 family members are known tumor suppressors that regulate the terminal differentiation and apoptosis, and the downregulation of let-7 has been directly associated with the upregulation of a key oncogene, RAS, in lung cancer [25]. Zhao demonstrated that cell invasion and migration were suppressed by the ectopic expression of let-7c in cells with a relatively high degree of metastasis, and cell migration and invasion were accelerated by the suppression of let-7c in relatively low metastatic cells, indicating that let-7c inhibits the migration and invasion of NSCLC cells [26]. Let-7c-5p acts as a tumor suppressor by inhibiting proliferation and promoting apoptosis in breast cancer cells [27]. These results revealed that the overexpression of let-7c-5p is a biomarker of NSCLC. In our study, the overexpression of let-7c-5p was significantly associated with NSCLC prognosis, and let-7c-5p was found to regulate COL3A1, which was downregulated in the honokiol treatment group, as demonstrated by RT-qPCR analysis. COL3A1 encodes a fibrillar collagen that is expressed in extensible connective tissues, such as the skin, lungs, and vascular system. Reportedly, the expression of COL3A1 can be substantially reduced in idiopathic pulmonary fibrosis fibroblasts after treatment with a histone deacetylase inhibitor [28]. Moreover, the overexpression of COL3A1 is a poor prognostic factor in bladder cancer, and is associated with decreased overall survival in patients [29]. These findings were all consistent with the results of our bioinformatics analysis and subsequent experiments. As such, we concluded that the overexpression of let-7c-5p is a favorable indicator of NSCLC prognosis, which is likely to act via the downregulation of COL3A1.

The PI3K/AKT signaling pathway mediates several cellular processes involved in the development and progression of tumors, including cell proliferation, differentiation, and invasion [30]. Aberrant activation of the PI3K/AKT signaling pathway is a common genetic alteration in lung cancer, and is associated with a high histological

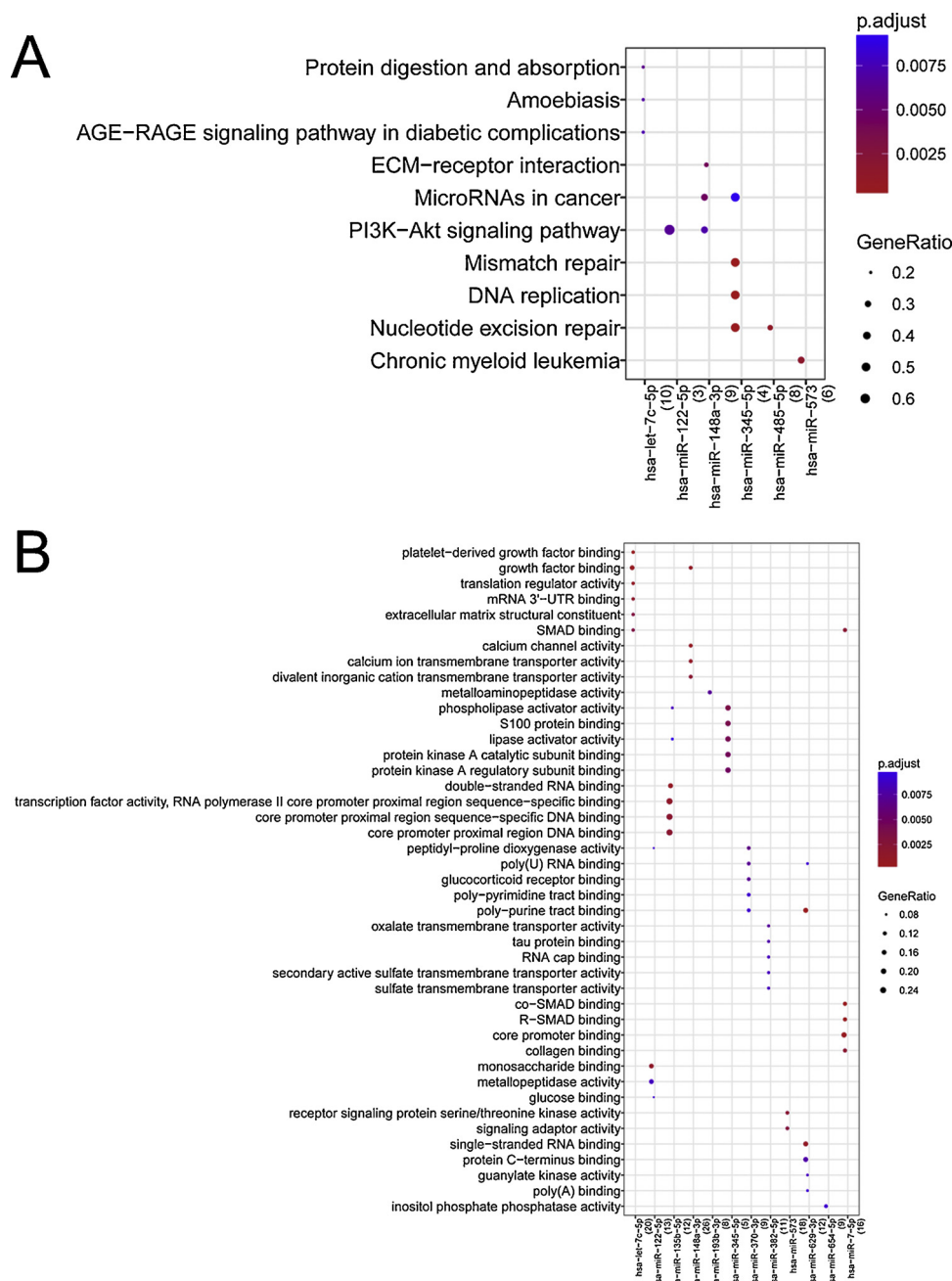


**Fig. 4.** Functional enrichment analysis for the DE-miRNAs. A: Significantly enriched KEGG pathways for DE-miRNAs. B: Significantly enriched GO annotations for DE-miRNAs.

grade and the more advanced cancer stages of NSCLC patients [31]. In this study, miR-148a-3p was significantly enriched in the PI3K/AKT signaling pathway and was associated with the target genes ERBB3 and ITGA5. Reportedly, the overexpression of miR-148a decreases cell growth and induces apoptosis in papillary thyroid cancer by suppressing PI3K and p-Akt protein expression in the PI3K/AKT signaling pathway [32]. The downregulation of the serum levels of miR-148a has been associated with advanced cancer stages and large tumor sizes in NSCLC patients [33]. In addition, it has been reported that miR-148a expression is suppressed in NSCLC metastatic samples, and miR-148a inhibits the metastasis and invasion of NSCLC both *in vitro* and *in vivo* [34]. Wang et al. indicated that miR-148a-3p inhibited the epithelial mesenchymal transition (EMT) and cell proliferation in bladder cancer via the regulatory circuits associated with ERBB3/AKT2/c-myc and DNMT1 [35]. A previous study confirmed that the overexpression of

miR-148a directly inhibited the expression of ERBB3 and the associated downstream signaling pathway involving AKT, ERK1/2, and p70S6K1 in breast cancer [36]. Cimino reported that miR-148b suppressed the progression of breast cancer by directly targeting ITGA5, which functions in the integrin signaling pathway [37]. Moreover, the overexpression of ITGA5 significantly decreased the overall survival rate of patients with node-negative NSCLC [38]. These results are in agreement with those of our own bioinformatics analysis and subsequent experiments. Hence, we suggest that miR-148a-3P and miR-148a-5P inhibit proliferation and migration, and induce apoptosis in NSCLC cells via the PI3K/AKT signaling pathway by targeting ERBB3 and ITGA5.

RB1 is the first reported tumor suppressor gene considered to be a negative regulator of the cell cycle [39]. Reportedly, RB1 is a direct target of miR-661, which promotes the metastasis and EMT of NSCLC cells [40]. Du reported that nicotine promoted the proliferation and

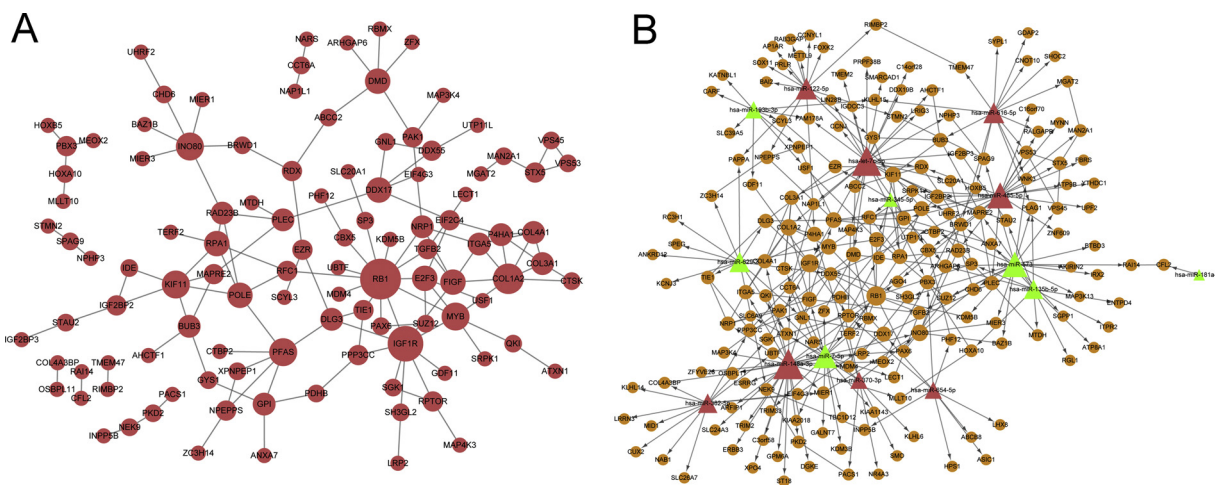


Fig. 5. Regulatory network involving DE-miRNAs and target mRNAs.

A: The protein-protein interaction network was constructed using DE-miRNAs-target genes. B: DE-miRNA-mRNA regulatory networks. Orange circles represent mRNAs, pink triangles represent upregulated DE-miRNAs, light green triangles represent downregulated DE-miRNAs, and arrows represent the DE-miRNA-mRNA interactions.

Table 1

The topology scores of the top 20 nodes in the PPI network.

mRNA	DC	mRNA	BC	mRNA	CC
RB1	11	RB1	2489.588	RB1	0.034706
IGF1R	9	IGF1R	1830.573	DLG3	0.034661
COL1A2	7	RAD23B	1658.008	IGF1R	0.034628
PFAS	6	RFC1	1577.265	POLE	0.034628
KIF11	6	POLE	1555.55	RFC1	0.034572
MYB	6	PFAS	1328.33	PFAS	0.034527
INO80	6	DLG3	1289.373	RPA1	0.034472
DMD	5	INO80	1059.043	MYB	0.034405
FIGF	5	MYB	1057.31	RAD23B	0.034218
POLE	5	PLEC	956.1667	TGFB2	0.03412
RPA1	5	KIF11	922.0762	FIGF	0.034098
DLG3	4	RPA1	908.3109	TIE1	0.034098
PLEC	4	NRP1	660.7727	EZR	0.034087
DDX17	4	COL1A2	651.0485	KIF11	0.034022
GPI	4	FIGF	629.5883	PPP3CC	0.03399
NRP1	4	DDX17	622	E2F3	0.033979
BUB3	4	RDX	568.6251	COL1A2	0.033861
ITGA5	4	DMD	561.3909	CBX5	0.03385
COL4A1	4	PAK1	546.0576	SP3	0.03385
RAD23B	4	EZR	484.6009	PAX6	0.03385

EMT of NSCLC cells by inducing miR-99b and miR-192 expression, which directly upregulated their target genes, fibroblast growth factor receptor 3 and RB1 [41]. In this study, RB1 was found to be the hub gene with the greatest degree of interaction in the PPI network, and was regulated by miR-7-5P. MiR-7-5p overexpression suppresses proliferation and triggers apoptosis in breast cancer cells by directly blocking the downstream target gene, proteasome activator subunit 3 [42]. It has been reported that miR-7-5p inhibits the microvascular endothelial cell proliferation of glioblastoma by regulating one of its target genes, Raf-1 Proto-Oncogene, Serine/Threonine Kinase [43]. Our findings suggest that RB1 may be a downstream target gene of miR-7-5p, and that miR-7-5p may inhibit the proliferation of NSCLC cells by targeting RB1.

5. Conclusion

In summary, miRNAs let-7c-5p, miR-148a-5p, miR-148a-3p, and miR-7-5p are potential biomarkers of honokiol-treated NSCLC cells. miR-148a-5p and miR-148a-3p inhibited proliferation and migration, and induced apoptosis in NSCLC cells, most likely via the PI3K/AKT signaling pathway by targeting ERBB3 and ITGA5. Let-7c-5p and miR-7-5p may act as tumor suppressors by targeting COL3A1 and RB1, respectively.

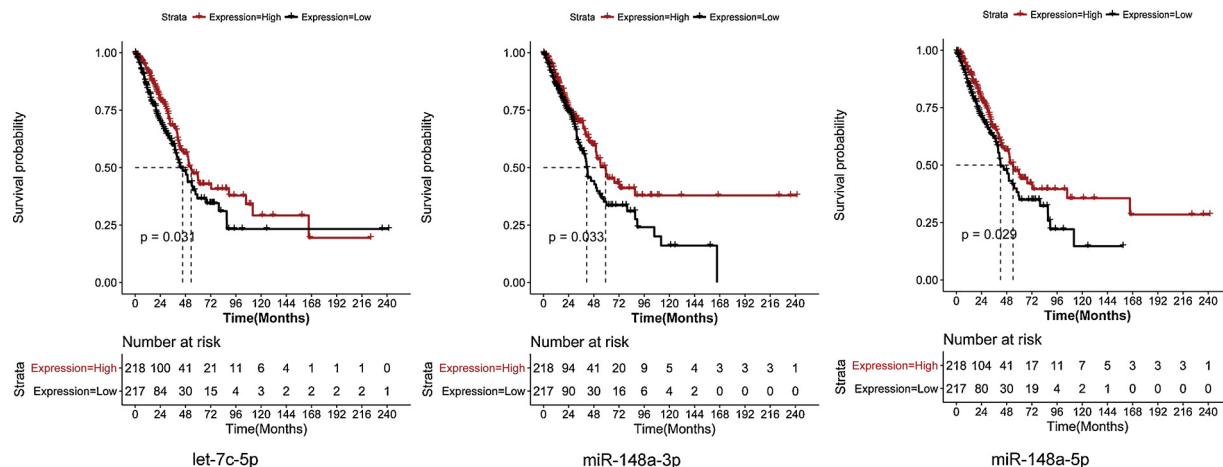
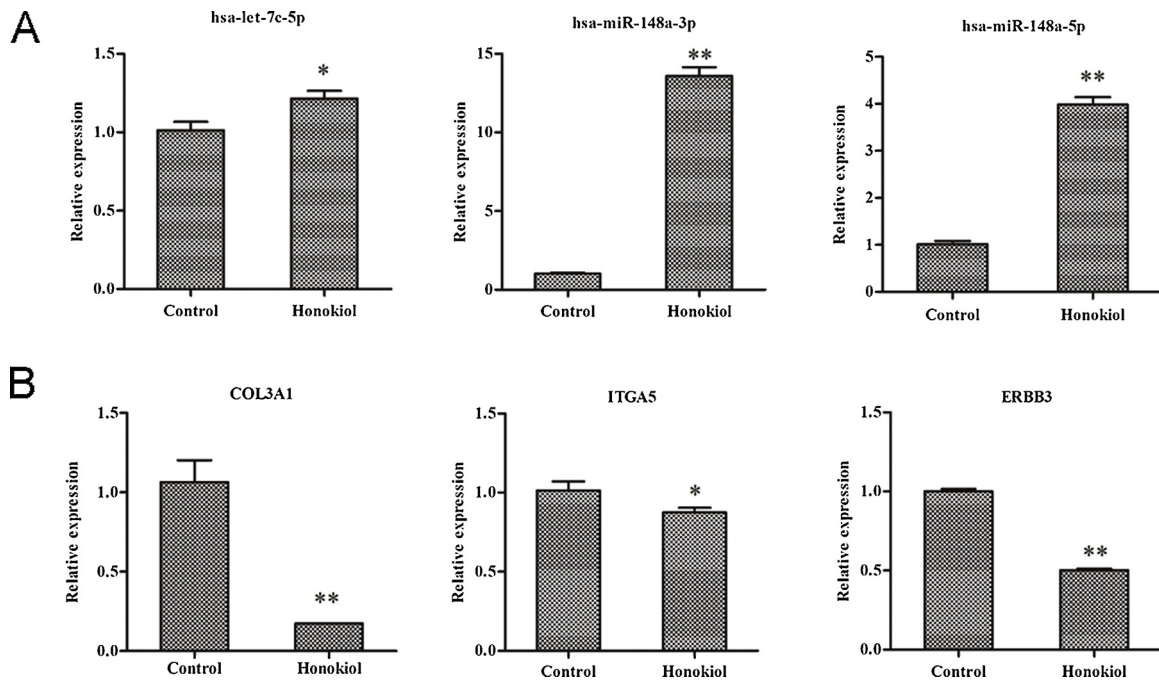
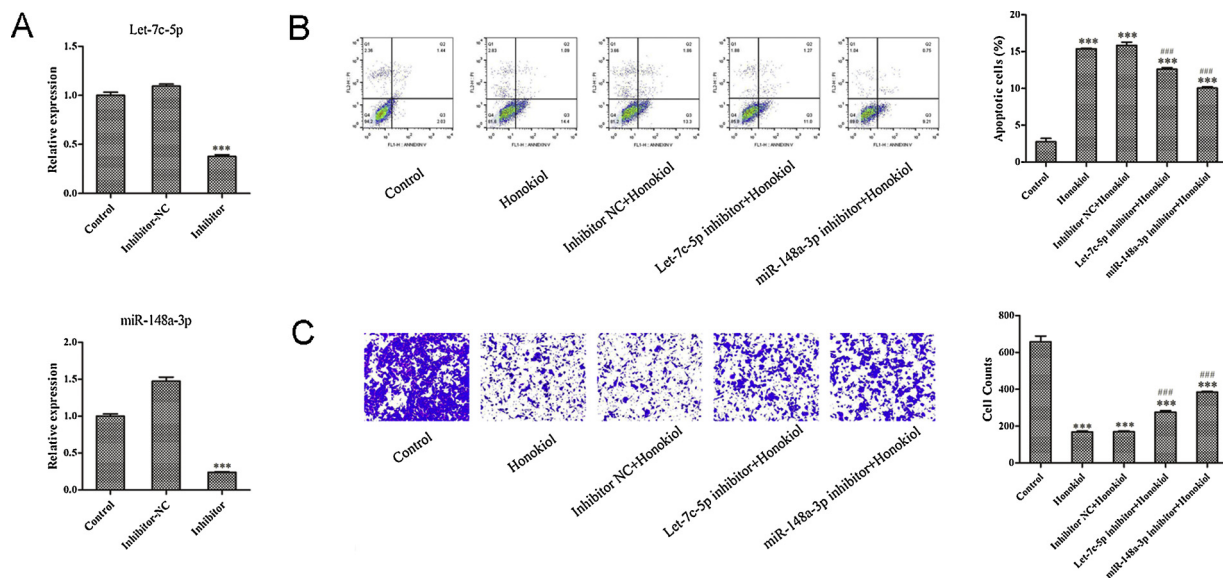


Fig. 6. Survival analysis based on DE-miRNAs.

A: Survival analysis with respect to let-7c-5p. B: Survival analysis with respect to miR-148a-5p. C: Survival analysis with respect to miR-148a-3p.



**Fig. 7.** Validation of the expression of DE-miRNAs and their target genes using RT-qPCR. A: The expression levels of let-7c-5p, miR-148a-5p, and miR-148a-3p were significantly increased in the honokiol group compared with those in the control group (let-7c-5p,  $P < 0.05$ ; miR-148a-5p and miR-148a-3p,  $P < 0.01$ ). B: The expression levels of COL3A1, ITGA5, and ERBB3 were significantly decreased in the honokiol group compared with those in the control group (ITGA5,  $P < 0.05$ ; COL3A1 and ERBB3,  $P < 0.01$ ).



**Fig. 8.** Let-7c-5p and miR-148a-3p inhibitors reversed the cytological effects of honokiol. A: The expression levels of let-7c-5p and miR-148a-3p were significantly decreased by their corresponding miRNA inhibitors ( $P < 0.001$ ). B: Flow cytometry determined the apoptosis of A549 cells, and the apoptosis induced by honokiol was partly reversed by the miRNA inhibitors ( $P < 0.001$ ). C: Transwell assay determined the migration of A549 cells, where the migration inhibited by honokiol was partly reversed by the miRNA inhibitors ( $P < 0.001$ ).

**Conflict of interest**

We declare that they have no competing interests.

**Acknowledgments**

This work was supported by The Affiliated Huai'an Hospital of Xuzhou Medical University.

**References**

- [1] R.S. Herbst, J.V. Heymach, S.M. Lippman, Lung cancer, *N. Engl. J. Med.* 359 (2008) 1367–1380.
- [2] Y. Jin, H. Xu, C. Zhang, et al., Combined effects of cigarette smoking, gene polymorphisms and methylations of tumor suppressor genes on non small cell lung cancer: a hospital-based case-control study in China, *BMC Cancer* 10 (2010) 1 (2010-08-12), 10: 422.
- [3] L.A. Torre, R.L. Siegel, J. Ahmedin, Lung cancer statistics, *Adv. Exp. Med. Biol.* 893 (2016) 1–19.
- [4] N. Yanaihara, N. Caplen, E. Bowman, et al., Unique microRNA molecular profiles in lung cancer diagnosis and prognosis, *Cancer Cell* 9 (2006) 189–198.
- [5] J.F. Barger, S.P. Nana-Sinkam, MicroRNA as tools and therapeutics in lung cancer,

- Respir. Med. 109 (2015) 803–812.
- [6] Q.Z. Wang, W.N. Xu, Potential uses of microRNA in lung cancer diagnosis, prognosis, and therapy, *Curr. Cancer Drug Targets* (2009) 9:–.
- [7] R. Charkiewicz, L. Pilz, A. Sulewska, et al., Validation for histology driven diagnosis in non-small cell lung cancer using hsa-mir-205 and hsa-mir-21 expression by two different normalization strategies, *Int. J. Cancer* 138 (2016) 689–697.
- [8] A. Markou, E.G. Tsaroucha, L. Kaklamani, M. Fotinou, V. Georgoulas, E.S. Lianidou, Prognostic value of mature microRNA-21 and microRNA-205 over-expression in non-small cell lung cancer by quantitative real-time rt-pcr, *Clin. Chem.* 54 (2008) 1696–1704.
- [9] J. Wei, W. Gao, C.J. Zhu, et al., Identification of plasma microRNA-21 as a biomarker for early detection and chemosensitivity of non-small cell lung cancer, *Chin. J. Cancer* 30 (2011) 407–414.
- [10] Z. Qi, D.Y. Yang, J. Cao, Increased micro-rna 17, 21, and 192 gene expressions improve early diagnosis in non-small cell lung cancer, *Med. Oncol.* 31 (2014) 195.
- [11] L. Xiang-Hua, L. Kai-Hua, W. Ke-Ming, et al., MicroRNA-196a promotes non-small cell lung cancer cell proliferation and invasion through targeting hoxa5, *BMC Cancer* 12 (348) (2012).
- [12] L.E. Fried, J.L. Arbiser, Honokiol, a multifunctional antiangiogenic and antitumor agent, *Antioxid. Redox Signal.* 11 (2009) 1139–1148.
- [13] H.E. Pearson, M. Iida, R.A. Orbuch, et al., Overcoming resistance to cetuximab with honokiol, a small-molecule polyphenol, *Mol. Cancer Ther.* (2017) 17.
- [14] T. Singh, R. Prasad, S.K. Katiyar, Inhibition of class I histone deacetylases in non-small cell lung cancer by honokiol leads to suppression of cancer cell growth and induction of cell death in vitro and in vivo, *Epigenetics* 8 (2013) 54–65.
- [15] L.X. Luo, Y. Li, Z.Q. Liu, et al., Honokiol induces apoptosis, G1 arrest, and autophagy in kras mutant lung cancer cells, *Front. Pharmacol.* 8 (199) (2017).
- [16] B. Langmead, C. Trapnell, M. Pop, S.L. Salzberg, Ultrafast and memory-efficient alignment of short DNA sequences to the human genome, *Genome Biol.* 10 (2009) R25.
- [17] M.I. Love, W. Huber, S. Anders, Moderated estimation of fold change and dispersion for RNA-seq data with DESeq2, *Genome Biol.* 15 (550) (2014).
- [18] H. Ogata, S. Goto, K. Sato, W. Fujibuchi, H. Bono, M. Kanehisa, Kegg: Kyoto encyclopedia of genes and genomes, *Nucleic Acids Res.* 27 (2000) 29–34.
- [19] T.G.O. Consortium, M. Ashburner, C.A. Ball, et al., Gene ontology: tool for the unification of biology, *Nat. Genet.* 25 (2000) 25–29.
- [20] S. Damian, F. Andrea, W. Stefan, et al., String v10: protein-protein interaction networks, integrated over the tree of life, *Nucleic Acids Res.* 43 (2015) D447.
- [21] P. Shannon, A. Markiel, O. Ozier, et al., Cytoscape: a software environment for integrated models of biomolecular interaction networks, *Genome Res.* 13 (2498) (2003).
- [22] Y. Tang, M. Li, J. Wang, Y. Pan, F.X. Wu, Cytoscape: a cytoscape plugin for centrality analysis and evaluation of protein interaction networks, *Biosystems* 127 (2015) 67–72.
- [23] C. Tyner, G.P. Barber, J. Casper, et al., The UCSC genome browser database: 2017 update, *Nucleic Acids Res.* (45) (2017) D626–D634.
- [24] K.J. Livak, T.D. Schmittgen, Analysis of relative gene expression data using real-time quantitative PCR and the 2<sup>-ΔΔC<sub>T</sub></sup> method, *Methods* 25 (2001) 402–408.
- [25] D. Barh, R. Malhotra, B. Ravi, P. Sindhurani, MicroRNA let-7: an emerging next-generation cancer therapeutic, *Curr. Oncol.* 17 (2010) 70–80.
- [26] B. Zhao, H. Han, J. Chen, et al., MicroRNA let-7c inhibits migration and invasion of human non-small cell lung cancer by targeting itgb3 and map4k3, *Cancer Lett.* 342 (2014) 43–51.
- [27] X. Fu, X. Mao, Y. Wang, X. Ding, Y. Li, Let-7c-5p inhibits cell proliferation and induces cell apoptosis by targeting ERCC6 in breast cancer, *Oncol. Rep.* (2017) 38.
- [28] X. Zhang, H. Liu, T. Hock, V.J. Thannickal, Y.Y. Sanders, Histone deacetylase inhibition downregulates collagen 3a1 in fibrotic lung fibroblasts, *Int. J. Mol. Sci.* 14 (2013) 19605–19617.
- [29] L. Yuan, B. Shu, L. Chen, et al., Overexpression of COL3A1 confers a poor prognosis in human bladder cancer identified by co-expression analysis, *Oncotarget* 8 (2017) 70508–70520.
- [30] C. Fumarola, M.A. Bonelli, P.G. Petronini, R.R. Alfieri, Targeting PI3K/AKT/mTOR pathway in non-small cell lung cancer, *Biochem. Pharmacol.* 90 (2014) 197–207.
- [31] M. Scrima, C. De Marco, F. Fabiani, et al., Signaling networks associated with AKT activation in non-small cell lung cancer (NSCLC), *PLoS One* 7 (2012) e30427.
- [32] Y. Xu, Y.F. Han, S.J. Zhu, J.D. Dong, B. Ye, Mirna148a inhibits cell growth of papillary thyroid cancer through STAT3 and PI3K/AKT signaling pathways, *Oncol. Rep.* 38 (3085) (2017).
- [33] Y. Jin-Shan, L. Bao-Jian, L. Hua-Wei, et al., Serum mir-152, mir-148a, mir-148b, and mir-21 as novel biomarkers in non-small cell lung cancer screening, *Tumour Biol.* 36 (2015) 3035–3042.
- [34] L. Jing, Y. Tao, L. Lei, et al., MicroRNA-148a suppresses invasion and metastasis of human non-small-cell lung cancer, *Cell. Physiol. Biochem.* 37 (2015) 1847–1856.
- [35] W. Xiao, L. Zhen, X. Xin, et al., Mir-148a-3p represses proliferation and EMT by establishing regulatory circuits between ERBB3/AKT2/c-myc and DNMT1 in bladder cancer, *Cell Death Dis.* 7 (2016) e2503.
- [36] Qing Jing, Jiang Binghua, Mir-148a inhibits angiogenesis by targeting ERBB3, *J. Biomed. Res.* 25 (2011) 170–177.
- [37] D. Cimino, C.D. Pittà, F. Orso, et al., Mir148b is a major coordinator of breast cancer progression in a relapse-associated microRNA signature by targeting ITGA5, ROCK1, PIK3CA, NRAS, and CSF1, *FASEB J.* 27 (2013) 1223–1235.
- [38] M. Adachi, T. Taki, M. Higashiyama, N. Kohno, H. Inufusa, M. Miyake, Significance of integrin alpha5 gene expression as a prognostic factor in node-negative non-small cell lung cancer, *Clin. Cancer Res.* 6 (2000) 96–101.
- [39] M. Chinnam, D.W. Goodrich, Rb1, development, and cancer, *Curr. Top. Dev. Biol.* 94 (2011) 129–169.
- [40] F. Liu, Y. Cai, X. Rong, et al., Mir-661 promotes tumor invasion and metastasis by directly inhibiting Rb1 in non-small cell lung cancer, *Mol. Cancer* 16 (122) (2017).
- [41] X. Du, F. Qi, S. Lu, Y. Li, W. Han, Nicotine upregulates FGFR3 and Rb1 expression and promotes non-small cell lung cancer cell proliferation and epithelial-to-mesenchymal transition via downregulation of mir-99b and mir-192, *Biomed. Pharmacother.* 101 (2018) 656–662.
- [42] Y. Shi, X. Luo, P. Li, et al., Mir-7-5p suppresses cell proliferation and induces apoptosis of breast cancer cells mainly by targeting REGY, *Cancer Lett.* 358 (2015) 27–36.
- [43] Z. Liu, Y. Liu, L. Li, et al., Mir-7-5p is frequently downregulated in glioblastoma microvasculature and inhibits vascular endothelial cell proliferation by targeting RAFL1, *Tumor Biol.* 35 (2014) 10177–10184.